

# Analyses of acoustic streaming field in the probe-liquid-substrate system for nanotrapping

Qiang Tang<sup>1</sup> · Junhui Hu<sup>1</sup>

Received: 3 June 2015 / Accepted: 14 September 2015 / Published online: 9 November 2015  
© Springer-Verlag Berlin Heidelberg 2015

**Abstract** The probe-liquid-substrate system, in which a micro-manipulation probe (MMP) is inserted into a liquid film of nanosuspension on a substrate, is very useful in nanomanipulations. With the MMP's vibration, a three-dimensional (3D) acoustic streaming field around the MMP is generated, which has been used to trap, transfer and rotate nanoentities in the liquid film. However, research on the details of the 3D acoustic streaming field in the probe-liquid-substrate system has been scarce. In this work, the 3D acoustic streaming field in a probe-liquid-substrate system for the contact-type trapping of individual nanowires is numerically investigated by the finite element method. The computational results show that the MMP root's elliptical vibration can generate an acoustic streaming field capable of trapping a single nanowire in the contact mode. This conclusion can well explain the experimental phenomena that the MMP can trap a single nanowire at some frequencies and cannot at others. The computational results clarify the effect of the distance between the MMP and substrate, the MMP's radius and length, and the water film's thickness on the acoustic streaming field.

**Keywords** Probe-liquid-substrate system · Acoustic streaming · Nanotrapping · Elliptical vibration

## 1 Introduction

The manipulation of nanoobjects by ultrasound has potential applications in the micro-/nanoassembly, nanomeasurement, fabrication of high-end sensors, etc. (Hu 2014; Li et al. 2010; Li and Hu 2014a, b; Balk et al. 2014; Ahmed et al. 2014). The probe-liquid-substrate system (Hu 2014), in which a micro-manipulation probe (MMP) is inserted into a liquid film of nanosuspension on a substrate, has been demonstrated to be very useful in the ultrasonic nanomanipulations such as contact-type and noncontact-type trapping of a single nanowire (Li et al. 2010; Li and Hu 2014a), and rotary driving of a single nanowire (Li and Hu 2014b). It uses acoustic streaming eddies in a 3D acoustofluidic field generated by and around the MMP to implement the nanomanipulation functions. The acoustic streaming eddies have a fixed relative position to the MMP. Thus, it can be moved by tuning the position of the MMP or ultrasonic transducer, which allows the transfer of trapped objects (Li et al. 2010; Li and Hu 2014a, b). One of the merits of ultrasonic manipulations based on the probe-liquid-substrate system is that the temperature rise can be very small ( $<0.1$  °C) at the manipulation area (Hu 2014; Li and Hu 2014b).

There was little to no in-depth research on the 3D acoustic streaming field in the probe-liquid-substrate system before this work, and this is hindering the optimization design and applications of the probe-liquid-substrate system in the nanomanipulation. In our ultrasonic nanomanipulation based on the probe-liquid-substrate system, the acoustic streaming field around an MMP is observed under microscope by using micro-/nanomarkers scattered in the suspension film (Li et al. 2010; Li and Hu 2014a, b). Owing to the geometrical typologies of the devices, the

---

✉ Junhui Hu  
ejhhu@nuaa.edu.cn

<sup>1</sup> State Key Lab of Mechanics and Control of Mechanical Structures, Nanjing University of Aeronautics and Astronautics, Nanjing 210016, China

acoustic streaming fields obtained are usually incomplete. Also, the typologies of acoustofluidic fields in the existing computational models are quite different from that in the probe-liquid-substrate system (Muller et al. 2012, 2013; Lei et al. 2014; Nama et al. 2014; Wada et al. 2014; Sundin et al. 2007; Devendran et al. 2014). Thus, the theoretical results based on these computational models cannot be applied to an analysis of the acoustic streaming field in the probe-liquid-substrate system.

In this work, we analyze the 3D acoustofluidic field in the probe-liquid-substrate system for the nanotrapping by a computational model, developed by our group. The computational results can well explain why the MMP can trap single nanowires at some frequencies and cannot at the others. The most important discovery in this work is that the MMP root's elliptical vibration can generate the acoustic streaming field capable of trapping a single nanowire in the contact mode (Li et al. 2010; Li and Hu 2014a). Moreover, our computation reveals that the manipulation capability of the probe-liquid-substrate system is influenced by the parameters such as the distance between the MMP and substrate, the MMP's radius and length, and the liquid film's thickness. The dependency of the acoustic streaming field around the MMP on these parameters is clarified quantitatively.

## 2 Computational model and method

A math-physical model for the probe-liquid-substrate system is shown in Fig. 1a, and its meshed FEM model is shown in Fig. 1b. To take a balance between the computational error and time, the mesh size of the acoustofluidic field near the MMP is smaller than that in the rest region of the acoustofluidic field. Within the region enclosed by a cylindrical surface with a radius of  $2R_p \sim 3R_p$  for most of the computational work, in which  $R_p$  is the MMP's radius, the maximum element size is  $1.5 \mu\text{m}$  (30 % of the MMP's radius and about 0.0135 % of the wavelength of the sound field at 135 kHz). In the rest region of the acoustofluidic, the maximum element size is  $0.55 \text{ mm}$  (4.95 % of the wavelength of the sound field at 135 kHz). Also, the maximum element size in the MMP is  $0.2 \text{ mm}$ .

The boundary conditions of the probe-liquid-substrate system for the sound field and acoustic streaming in the liquid film are shown in Fig. 2. The computation of the acoustic streaming field is implemented by the finite element method (FEM) software COMSOL Multiphysics (version 4.3a). In this work, only the steady-state acoustic streaming field is computed. The computational process consists of the following three steps.

In the first step, the sound field is solved by the sound-structure coupling module with the boundary conditions

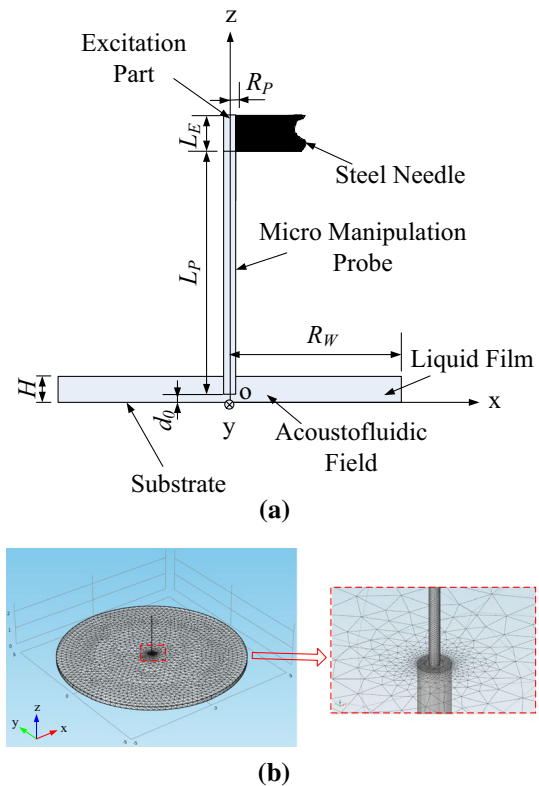


**Fig. 1** (color online). 3D model and meshing for the probe-liquid-substrate system. **a** Math-physical model for the acoustofluidic field. **b** Meshed model for the acoustofluidic field

shown in Fig. 2a. Boundary conditions of the sound field are as follows: The acceleration is continuous at the interfaces between the MMP and liquid film; the interfaces between the water film and air are sound soft (sound pressure  $p = 0$ ) for the reason that ultrasound attenuates quickly in the air; the interface between the water film and substrate is sound hard ( $\frac{\partial p}{\partial n} = 0$ , where  $\mathbf{n}$  denotes the unit normal vector of the boundary). The following wave equation (Kinsler et al. 1999) is used to solve the sound field:

$$\rho \frac{\partial^2 p}{\partial t^2} = \rho c^2 \nabla^2 p + b \nabla \frac{\partial p}{\partial t} \quad (1)$$

where  $p$  is the sound pressure,  $\rho$  is the fluid density, and  $c$  is the sound speed, and the acoustic dissipation factor  $b$  is computed by

$$b = \frac{4}{3} \eta + \eta' \quad (2)$$

where  $\eta$  and  $\eta'$  are the shear and bulk viscosity coefficient of the acoustic medium, respectively.

In the second step, computed vibration velocity and sound pressure of the sound field are used to calculate the spatial gradients of the Reynolds stress and mean pressure (the second-order pressure in the sound field), by the

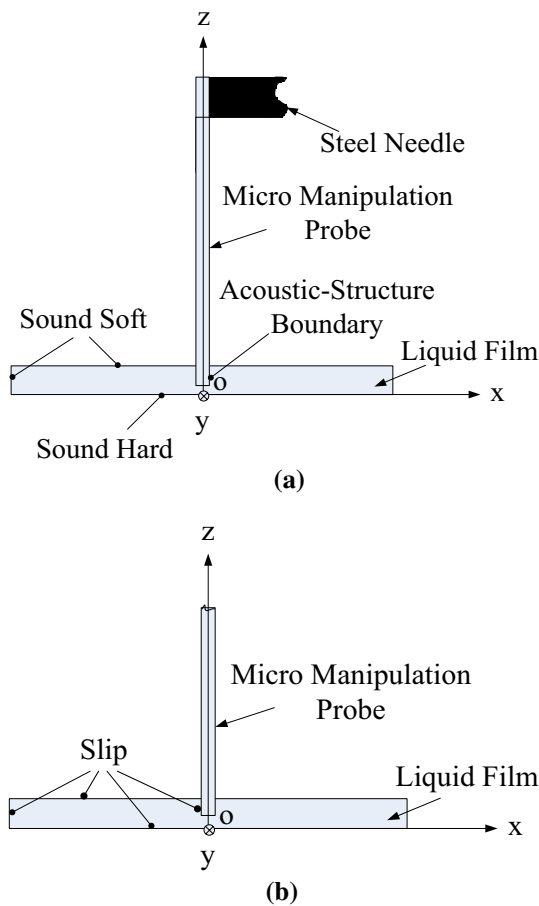


**Fig. 2** Boundary conditions of the acoustofluidic field. **a** Boundary conditions for the sound field. **b** Boundary conditions for the acoustic streaming field

postprocessing functions of the FEM software. The spatial gradients of the Reynolds stress and mean pressure are the force generating the acoustic streaming. The spatial gradient of the Reynolds stress  $F_j$  is computed by (Tang and Hu 2015; Lighthill 1978)

$$F_j = -\partial(\overline{\rho_0 u_i u_j})/\partial x_i \tag{3}$$

where  $\rho_0$  is the medium density in the undisturbed state,  $u_i$  is the vibration velocities of the sound field, repeated suffix  $i$  and  $j$  represent  $x$ ,  $y$  and  $z$  in the 3D model, and the symbol “ $\bar{\phantom{x}}$ ” signifies the mean value over one time period. The mean pressure  $\bar{p}_2$  is computed by (Tang and Hu 2015)

$$\bar{p}_2 = \frac{1}{2\rho_0 c_0^2} \frac{B}{A} \langle p_1^2 \rangle \tag{4}$$

where  $p_1$  represents the (first order) sound pressure,  $\langle \phantom{x} \rangle$  represents the time average over one time period,  $c_0$  is the medium sound speed in the undisturbed state, and  $\frac{B}{A}$  is the nonlinear parameter of the medium (Beyer 1965, 1997).

In the last step, the steady acoustic streaming is solved by the fluidic dynamics module of the FEM software. The steady acoustic streaming satisfies the following equation (Lighthill 1978):

$$\rho_0(\bar{u}_i \partial \bar{u}_j / \partial x_i) = F_j - \partial \bar{p}_2 / \partial x_j + \eta \nabla^2 \bar{u}_j \tag{5}$$

where  $\bar{u}_i$  is acoustic streaming velocity. The acoustic streaming also satisfies the continuity equation

$$\rho_0 \partial \bar{u}_i / \partial x_i = 0. \tag{6}$$

Slip boundary condition is used in the FEM computation of the acoustic streaming as shown in Fig. 2b. This is because our experiment shows that a tangential acoustic streaming can exist at the interface between the water film and substrate (Zhou et al. 2013).

### 3 Experimental verification

To experimentally verify the FEM simulation results, a probe-liquid-substrate system to trap a single silver nanowire in a water film on a silicon substrate is constructed. The experimental silver nanowires have a diameter of 100 nm and length of several microns up to several tens of microns. Figure 3a shows a photograph of the experimental setup. Figure 3b shows the detailed size and structure of the probe-liquid-substrate system with a transducer to excite the vibration of the system. An MMP that is mechanically excited by a steel needle is immersed into the nanowire suspension film on the substrate. The MMP is bonded on and excited by the tip of the steel needle, which is mechanically driven by a sandwich-type piezoelectric transducer shown in Fig. 3b. The steel needle is 25 mm long and 1 mm thick. The outer and inner diameters and the thickness of each piezoelectric ring in the transducer are 12, 6 and 1.2 mm, respectively. The piezoelectric constant  $d_{33}$  is  $250 \times 10^{-12}$  C/N, electromechanical coupling factor  $k_{33}$  is 0.63, mechanical quality factor  $Q_m$  is 500, dielectric dissipation factor  $\tan \delta$  is 0.6 %, and density is  $7450 \text{ kg/m}^3$ . The two stainless plates at the two ends of the transducer are square with 20 mm length and 2 mm thickness. The tightening torque applied to the transducer is 6 Nm. The resonance frequency of the sandwich transducer is 93 kHz, and the manipulation system with a working frequency of about 135 kHz is not at resonance.

The tip of the steel needle is used to excite the vibration of the MMP in the probe-liquid-substrate system. The amplitudes and initial phases of the three orthogonal vibration components at the tip of the steel needle are measured by a laser vibrometer (Polytec PSV-300 F). The distance between the MMP tip and substrate is controlled by an XYZ stage, and the water film thickness is controlled by

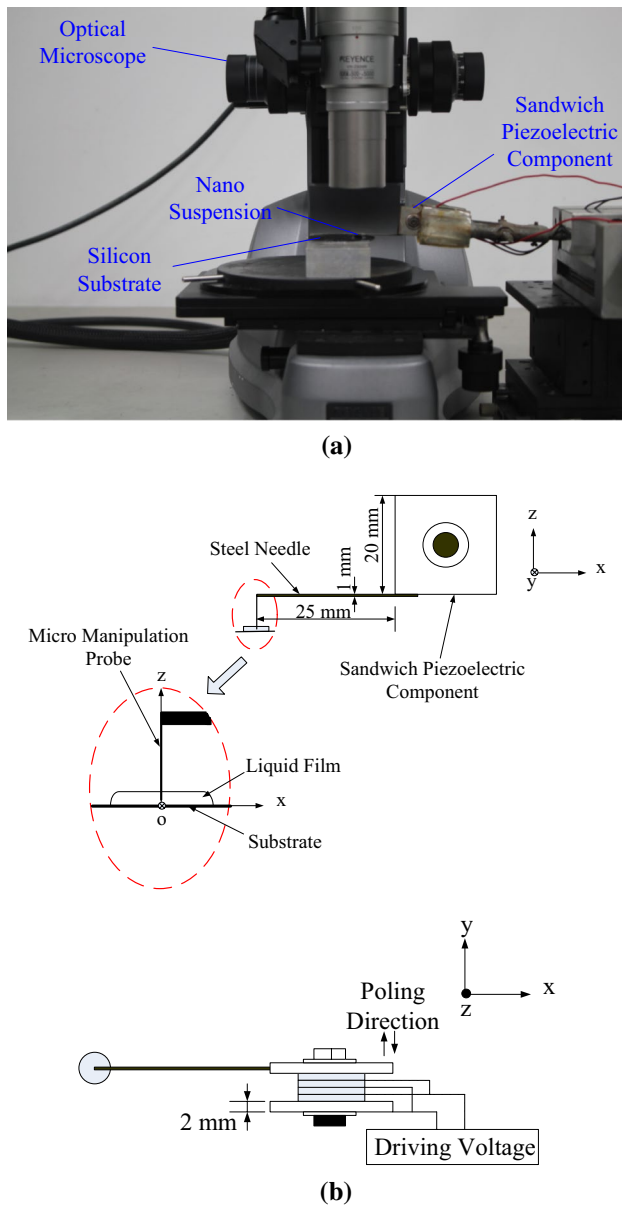


**Fig. 3** (color online). Experimental setup and the device to verify computational results. **a** Photograph of the experimental setup. **b** Device structure and size

**Table 1** Parameters of the probe-liquid-substrate system

The water film's thickness $H$ (mm)	The water film's radius $R_W$ (mm)	The MMP's length $L_p$ (mm)
0.2	5	1.5
The MMP's radius $R_p$ ( $\mu\text{m}$ )	The distance between MMP tip and substrate $d_0$ ( $\mu\text{m}$ )	The excited part length $L_E$ (mm)
5	5	1
Density of water $\rho$ ( $\text{kg}/\text{m}^3$ )	Speed of sound in water $c$ (m/s)	Shear viscosity of water $\eta$ (Pa s)
1000	1500	0.001
Volume-to-shear viscosity ratio in water $\eta'/\eta$	Nonlinear parameter of water at room temperature $\frac{B}{A}$	Density of MMP $\rho_p$ ( $\text{kg}/\text{m}^3$ )
2.1	5	2200
Young's modulus of MMP $E_p$ (Pa)	Shear modulus of MMP $G_p$ (Pa)	
$7.4 \times 10^{10}$	$2.846 \times 10^{10}$	

properly spreading out the water film and measuring its approximate height. Considering the evaporation during the experiments, the initial water film is thicker than  $200 \mu\text{m}$ . Actually, the trapping performance is not sensitive to the water film thickness as long as it is larger than  $50 \mu\text{m}$ .

## 4 Results and discussion

To simplify the computation, the sandwich transducer and the steel needle used to excite the MMP's vibration are not included in the FEM model of the probe-liquid-substrate system. Also, unless otherwise specified, property parameters of the MMP and the liquid film (water) shown in Table 1 (Liebermann 1949) are used.

Three orthogonal vibration components (the  $x$ ,  $y$  and  $z$  components in Fig. 3) at the MMP root were measured by the laser Doppler vibrometer (Polytec PSV-300 F) at the frequencies 125, 130, 135 and 140 kHz, and the results are shown in Table 2. The measured vibration information includes the vibration amplitude and initial phase. Also, the trapping performance at these frequencies was observed, and the results are also listed in Table 2. It shows that only at 135 kHz can the acoustic streaming field be used to trap a single nanowire. To explain the experimental phenomena, the acoustic streaming field around the MMP is computed, and flow patterns on the silicon substrate and in the  $yz$  plane (the plane that is perpendicular to the substrate and vibration transmission needle, and passes the center axis of the MMP) are shown in Figs. 4 and 5. Figure 4 shows the result for 135 kHz, and Fig. 5 the results for 125, 130 and 140 kHz. In the computation, the parameters listed in Table 2 were used, and the distance between the MMP tip and substrate was  $5 \mu\text{m}$ .

The trapping performance listed in Table 2 is explained by Figs. 4 and 5 as follows. From Fig. 4a, it is seen that a nanowire lying on the substrate surface within the effect range can be driven toward the point directly under the MMP tip from  $p1$  to  $p3$  through  $p2$ , by the inward flow along the  $y$  direction. Under the MMP tip, the sucked

**Table 2** Measured vibration distribution and workability at some frequencies

$f$ (kHz)	125	130	135	140
$A_x$ (nm)	17.45	9.44	5.77	13.72
$A_y$ (nm)	11.44	35.78	18.20	14.10
$A_z$ (nm)	6.11	18.54	15.68	9.69
$\Phi_x$ (°)	-100.0	-131.1	-134.5	100.0
$\Phi_y$ (°)	13.9	120.3	165	-23.3
$\Phi_z$ (°)	-144.9	-99.1	67.4	59.2
$\Phi_{zy} = \Phi_z - \Phi_y$ (°)	-158.8	-219.4	-97.6	82.5
$\Phi_{xy} = \Phi_x - \Phi_y$ (°)	-113.9	-251.4	-299.5	123.3
Can the device trap a single NW?	No	No	Yes	No

nanowire rotates to the  $x$  direction due to the  $\pm x$ -directional flow, while being lifted up by the upward flow (the  $z$ -directional flow), as shown in Fig. 4b. The lifted nanowire is pushed onto the MMP's side by the  $y$ -directional flow and aligned in the  $x$  direction by the  $\pm x$ -directional flow. Due to the pressing force on the trapped nanowire, there is a frictional force between the trapped nanowire and MMP, which contributes to the balance of the trapped nanowire.

The acoustic streaming shown in Fig. 5 can well explain why a single nanowire cannot be sucked to the MMP tip and trapped on the MMP at 125, 130 and 140 kHz. Images a1, b1 and c1 show that a single nanowire cannot reach a force balance under the MMP tip due to the severe asymmetry of the outward acoustic streaming, and it would be flushed away by the acoustic streaming on the substrate.

From the above discussion, it is known that the acoustic streaming shown in Figs. 4 and 5 can well explain why a single nanowire can be sucked to the MMP tip and trapped on the MMP at 135 kHz, and why it cannot be trapped at other frequencies, although the nanowire is not included in the FEM model. This indicates that the computed acoustic streaming field has the features which are needed to analyze the trapping performance, even if the nanowire is not included in the FEM model. This is because the diameter of the experimental nanowires is only 1/50 of the distance between the MMP tip and substrate.

The maximum acoustic streaming velocity on the silicon substrate surface is defined as  $V_{s,max}$  (see Fig. 4a), and the maximum  $z$ -directional velocity in the  $yz$  plane (see Fig. 4b), which is usually along the MMP wall, is defined as  $V_{l,max}$ . These two velocities are used to describe the strength of the acoustic streaming field in the following discussion.

To investigate the dependency of the acoustic streaming field on the phase difference among the orthogonal vibration components at the MMP root, the acoustic streaming field is computed with different phase difference values between the  $y$ - and  $z$ -directional vibration displacements

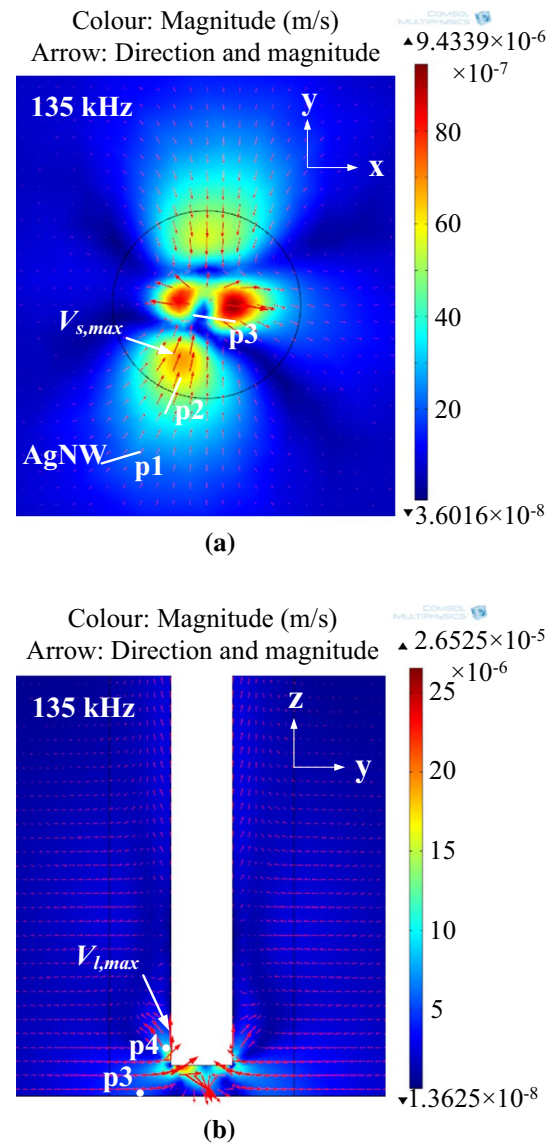


**Fig. 4** (color online). Acoustic streaming field on the substrate surface and in the  $yz$  plane (the plane that is perpendicular to the substrate and vibration transmission needle, and passes the center axis of the MMP) at 135 kHz. **a** Acoustic streaming field on the substrate. **b** Acoustic streaming field in the  $yz$  plane. The maximum acoustic streaming velocities on the substrate  $V_{s,max}$  and in the  $yz$  plane  $V_{l,max}$  are shown in **(a)** and **(b)**, respectively. The black circle in image **a**, representing the boundary between the fine and coarse element regions, has a radius of 15  $\mu\text{m}$ . And the white zone in image **b** representing the cross section of MMP has a width of 10  $\mu\text{m}$ . The separation between the MMP tip and substrate is 5  $\mu\text{m}$

$\Phi_{zy}$  at a working frequency of 130 kHz, and the computed results are shown in Fig. 6. In the computation, the amplitudes of the three orthogonal vibration displacement components and the phase difference values other than  $\Phi_{zy}$ , as listed in Table 2, are used, and all the computational parameters except  $\Phi_{zy}$  are kept constant to exclude the effects of

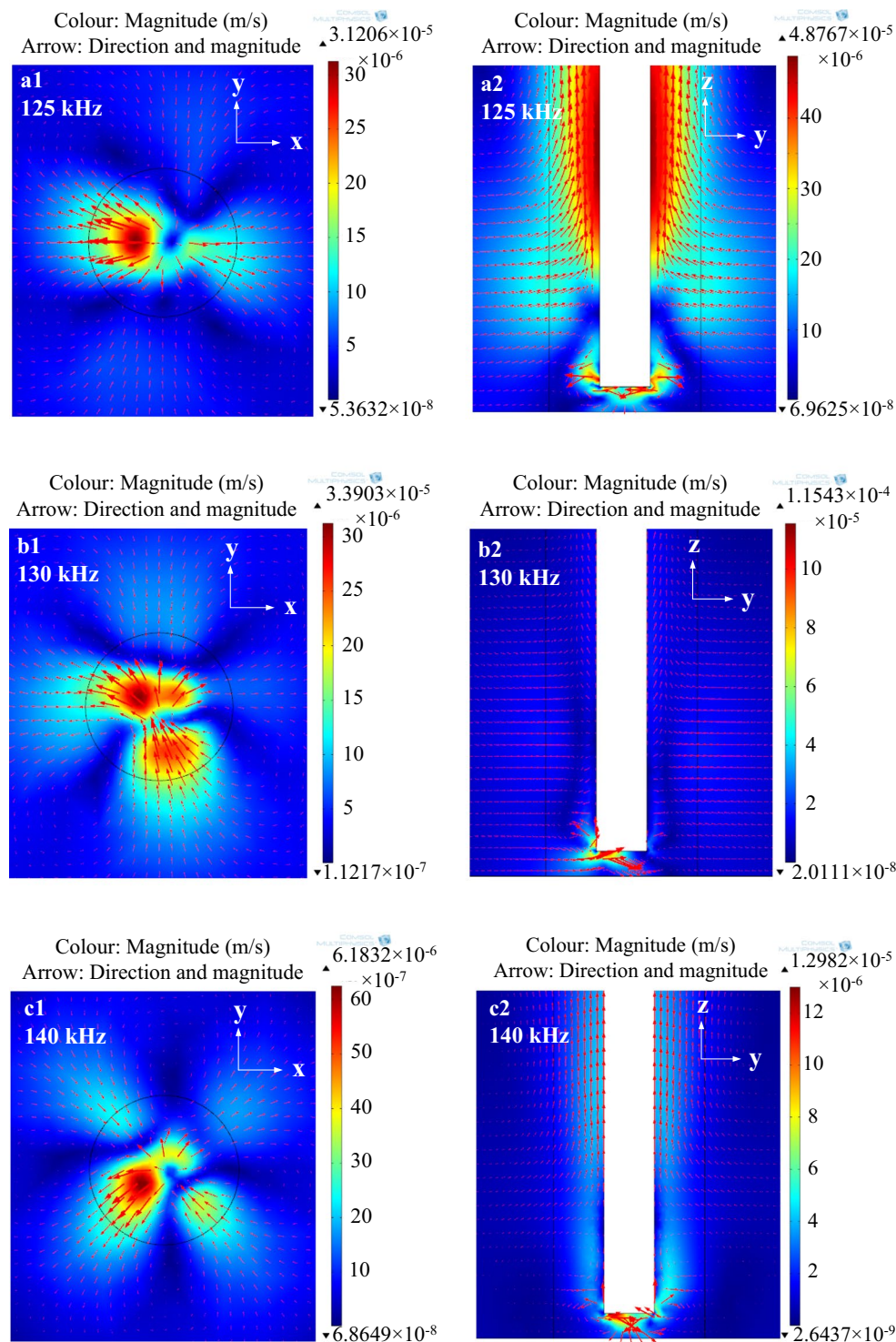


**Fig. 5** (color online). Acoustic streaming fields on the substrate surface and in the  $yz$  plane (the plane that is perpendicular to the substrate and vibration transmission needle, and passes the center axis of the MMP) at 125, 130 and 140 kHz. The *black circles* in images **a1**,

**b1** and **c1**, representing the boundary between the fine and coarse element regions, have a radius of  $15\ \mu\text{m}$ . And the *white zones* in images **a2**, **b2** and **c2**, representing the cross section of MMP, have a width of  $10\ \mu\text{m}$

these parameters. And the phase difference  $\Phi_{zy}$  is set to be  $0^\circ$ ,  $45^\circ$  and  $90^\circ$ . From images **a1**, **b1** and **c1** in Fig. 6, it is found that as the phase difference  $\Phi_{zy}$  increases, the

acoustic streaming pattern on the substrate becomes more symmetric about the  $x$ -axis, but the outward flow on the substrate remains asymmetric about the  $y$ -axis. For the

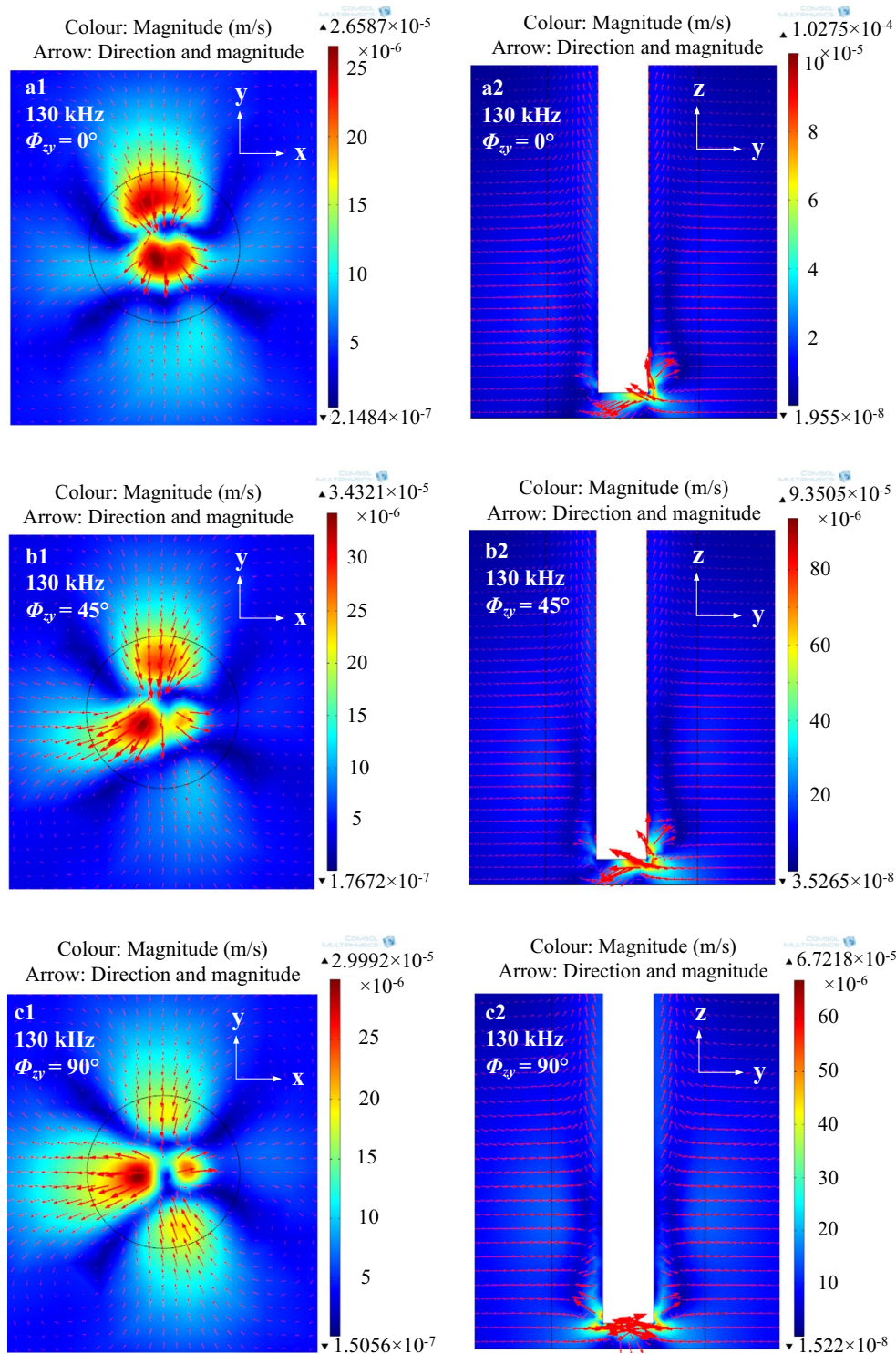
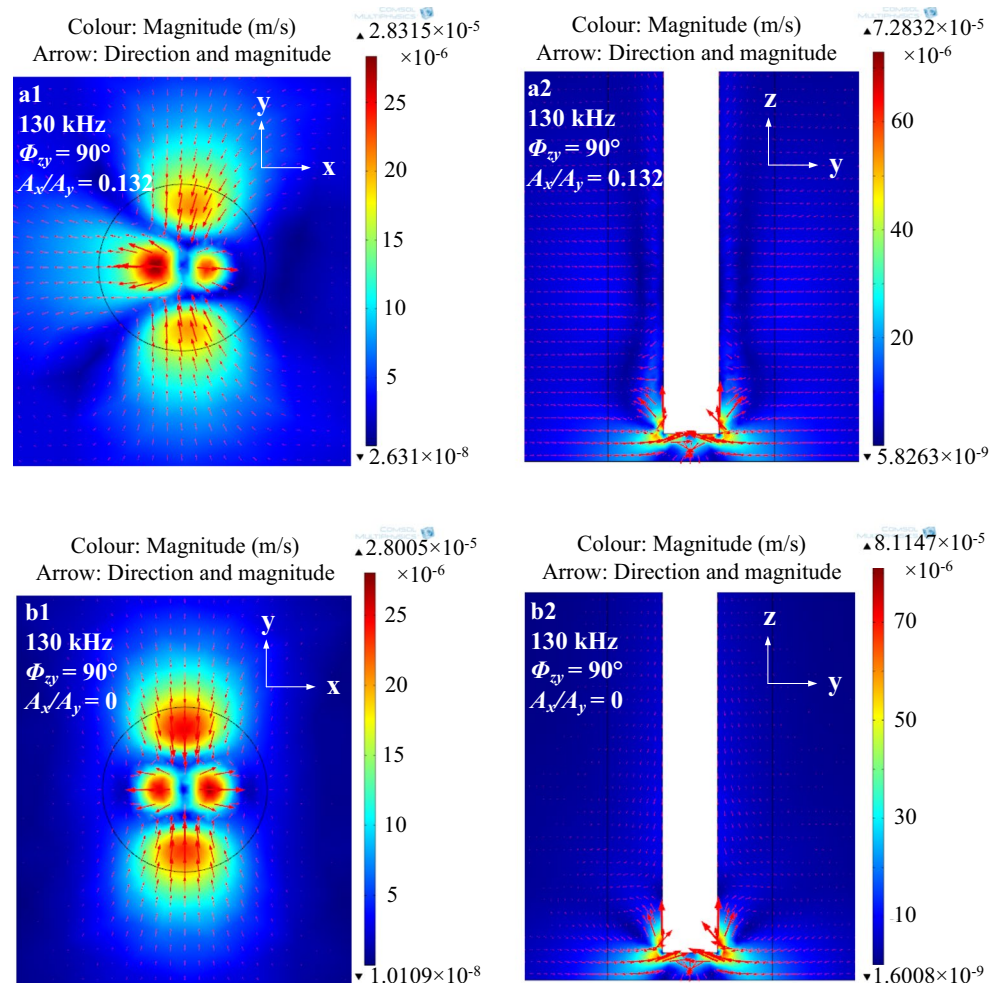


**Fig. 6** (color online). Acoustic streaming fields on the substrate surface and in the  $yz$  plane (the plane that is perpendicular to the substrate and vibration transmission needle, and passes the center axis of the MMP) at 130 kHz for different phase difference values between the  $y$ - and  $z$ -directional vibration displacement components  $\Phi_{zy}$  ( $=0^\circ$ ,

$45^\circ$  and  $90^\circ$ ). The *black circles* in images **a1**, **b1** and **c1**, representing the boundary between the fine and coarse element regions, have a radius of  $15 \mu\text{m}$ . And the *white zones* in images **a2**, **b2** and **c2**, representing the cross section of MMP, have a width of  $10 \mu\text{m}$

**Fig. 7** (color online). Acoustic streaming fields on the substrate surface and in the  $yz$  plane (the plane that is perpendicular to the substrate and vibration transmission needle, and passes the center axis of the MMP) at 130 kHz for different amplitude ratios between the  $x$ - and  $y$ -directional vibration displacement components  $A_x/A_y$  ( $=0.132$  and  $0$ ) when the phase difference between the  $y$ - and  $z$ -directional vibration displacement components is  $90^\circ$ . The *black circles* in images **a1** and **b1**, representing the boundary between the fine and coarse element regions, have a radius of  $15\ \mu\text{m}$ . And the *white zones* in images **a2** and **b2**, representing the cross section of MMP, have a width of  $10\ \mu\text{m}$



acoustic streaming field shown in image **c1**, it is still difficult for a sucked nanowire under the MMP tip to reach a force balance in the  $x$  direction.

In order to achieve a more symmetric acoustic streaming field which can be used to suck and trap a single nanowire, the acoustic streaming field at 130 kHz is computed for different amplitude ratio  $A_x/A_y$  at  $\Phi_{zy} = 90^\circ$ , and the results are shown in Fig. 7. In the computation,  $A_x$  decreases from  $9.44\ \text{nm}$  to  $0$ , and the other parameters are kept constant (see Table 2). The results shown in Fig. 7 indicate that as  $A_x/A_y$  decreases, the outward acoustic streaming becomes more symmetric about the  $y$ -axis, and a sucked and  $90^\circ$  rotated nanowire under the MMP tip can keep a force balance at  $A_x/A_y = 0$ .

Based on the results shown in Figs. 6 and 7, it comes to the conclusion that the MMP root's elliptical vibration in the  $yz$  plane can generate the acoustic streaming field capable of trapping a single nanowire in the contact mode. For this reason, the acoustic streaming field shown in Fig. 7b1, b2 is defined as the ideal flow field for the contact-type trapping of a single nanowire.

The effects of the distance between the MMP tip and substrate  $d_0$  on the acoustic streaming pattern and the maximum acoustic streaming velocities on the substrate and in the  $z$  direction, are computed at 135 kHz, and the results are shown in Fig. 8. Figure 8a shows the acoustic streaming patterns at  $d_0 = 2$  and  $8\ \mu\text{m}$ , and Fig. 8b the maximum acoustic streaming velocities on the substrate  $V_{s,\text{max}}$  and in the  $z$  direction  $V_{1,\text{max}}$  versus  $d_0$ . The computation shows that as the distance between the MMP tip and substrate increases, the acoustic streaming pattern on the substrate has a change, and the maximum acoustic streaming velocities on the substrate  $V_{s,\text{max}}$  and in the  $z$  direction  $V_{1,\text{max}}$  decrease. The decrease in  $V_{s,\text{max}}$  is because of the decrease in the tangential vibration velocity on the substrate as  $d_0$  increases. And the decrease in  $V_{1,\text{max}}$  is because the fluid circulates between the MMP tip and substrate as  $d_0$  increases. Therefore, a large distance between the MMP and substrate weakens the trapping capability.

The effect of the MMP's radius on the acoustic streaming field around the MMP was computed, and the results are shown in Fig. 9. In the computation, the working



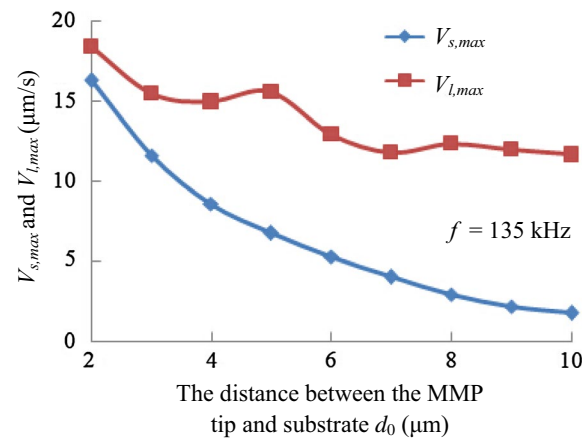
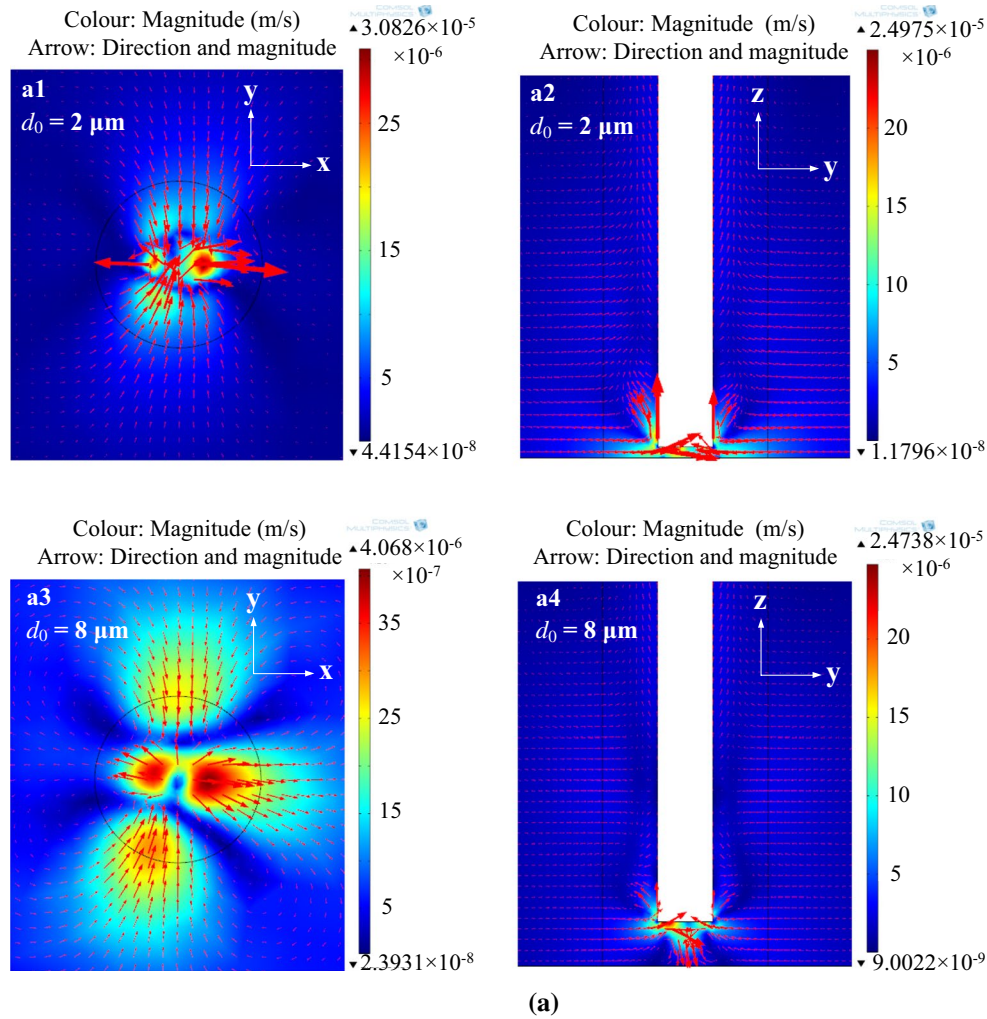


**Fig. 8** (color online). Acoustic streaming fields for different distance values between the MMP and substrate at 135 kHz. **a** Acoustic streaming patterns on the substrate surface and in the  $yz$  plane (the plane that is perpendicular to the substrate and vibration transmission needle, and passes the center axis of the MMP) at  $d_0 = 2$  and  $8 \mu\text{m}$ . **b** The maximum acoustic streaming velocities on the substrate sur-

face and in the  $yz$  plane versus the distance between the MMP and substrate. The *black circles* in images **a1** and **a3**, representing the boundary between the fine and coarse element regions, have a radius of  $15 \mu\text{m}$ . And the *white zones* in images **a2** and **a4**, representing the cross section of MMP, have a width of  $10 \mu\text{m}$

**Fig. 9** (color online). Acoustic streaming fields at different MMP's radii  $R_p$  at 135 kHz. **a** Acoustic streaming patterns on the substrate surface and in the  $yz$  plane (the plane that is perpendicular to the substrate and vibration transmission needle, and passes the center axis of the MMP) at  $R_p = 1, 8$  and  $12 \mu\text{m}$ . **b** The maximum acoustic streaming velocities on the substrate surface and in the  $yz$  plane versus the MMP's radius. The *black circles* in images **a1**, **a3** and **a5**, representing the boundary between the fine and coarse element regions, have a radius of 10, 15 and  $30 \mu\text{m}$ , respectively. And the *white zones* in images **a2**, **a4** and **a6**, representing the cross section of MMP, have a width of 2, 16 and  $24 \mu\text{m}$ , respectively

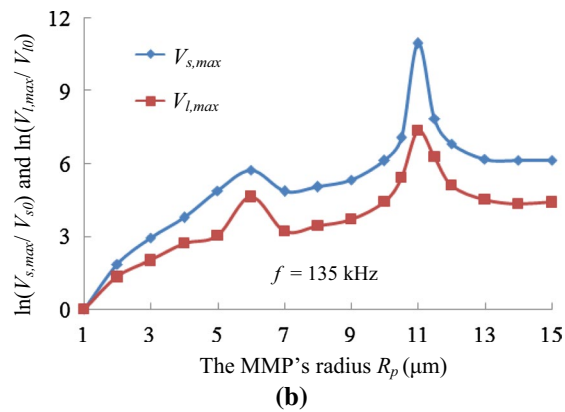
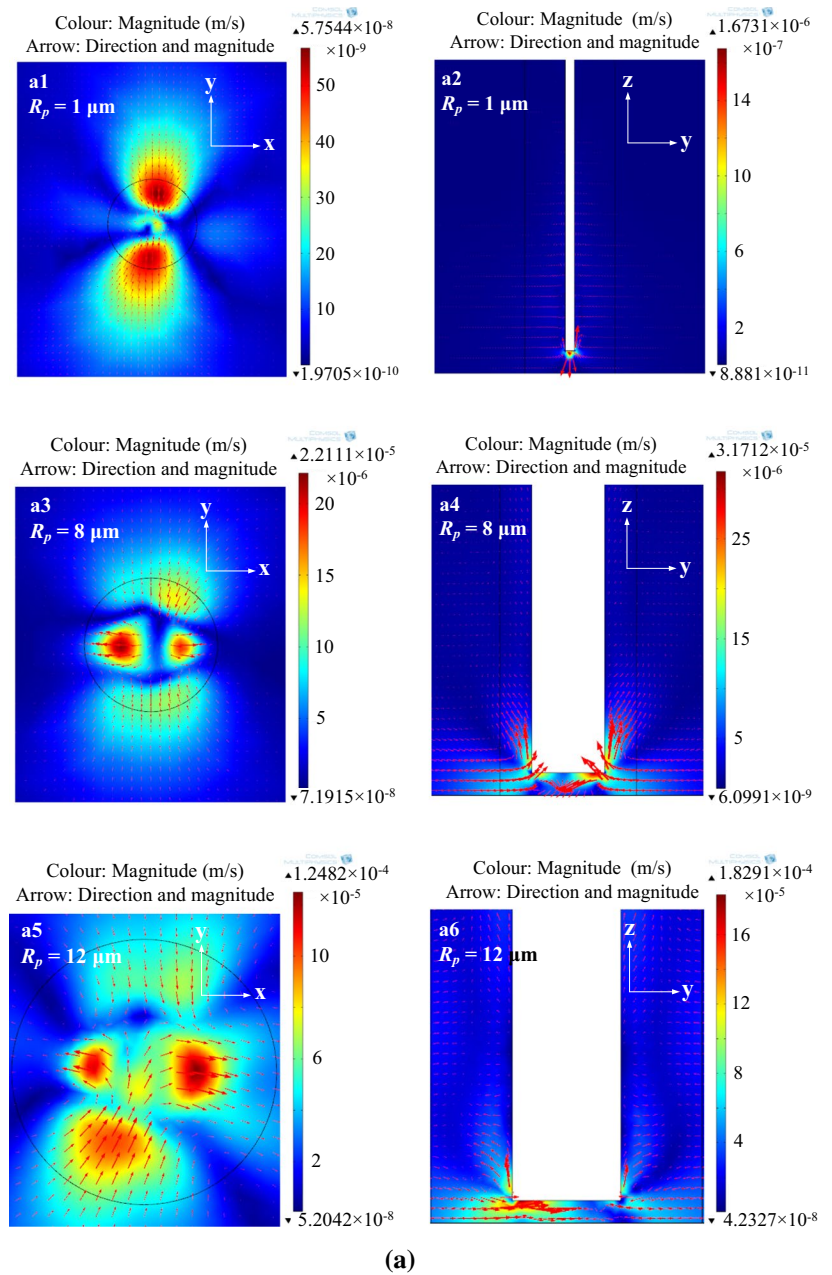
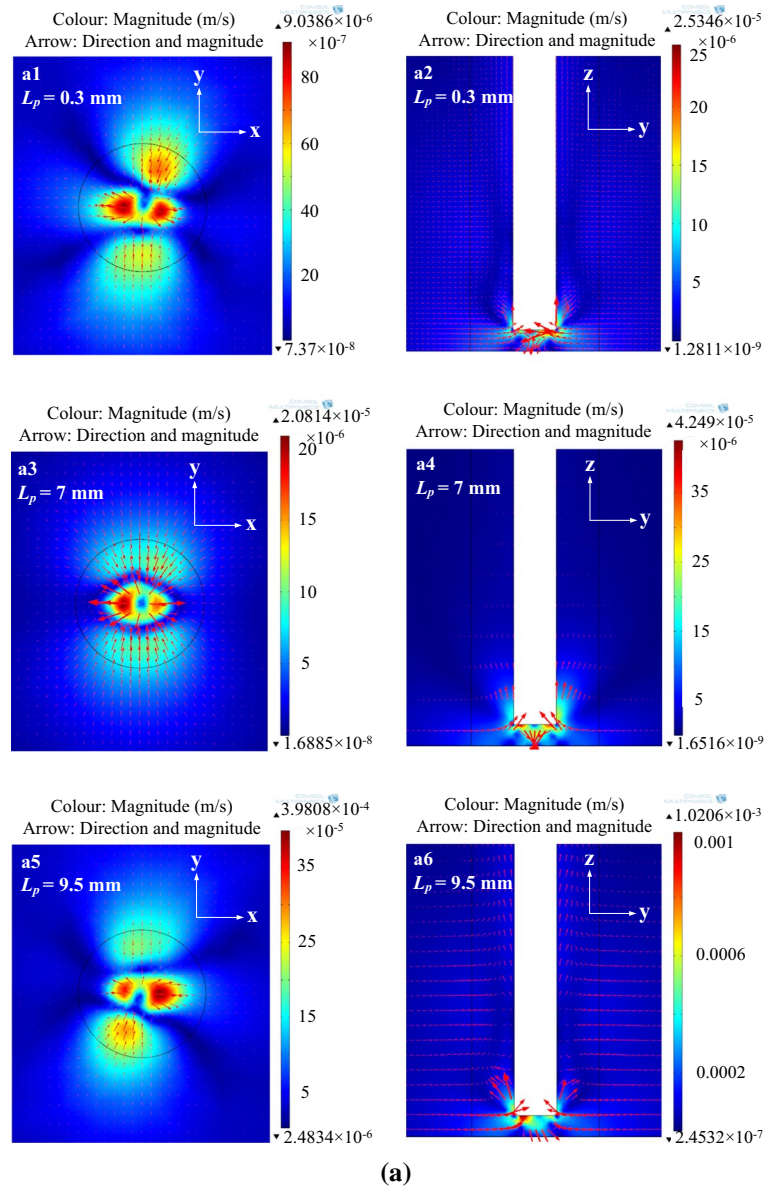
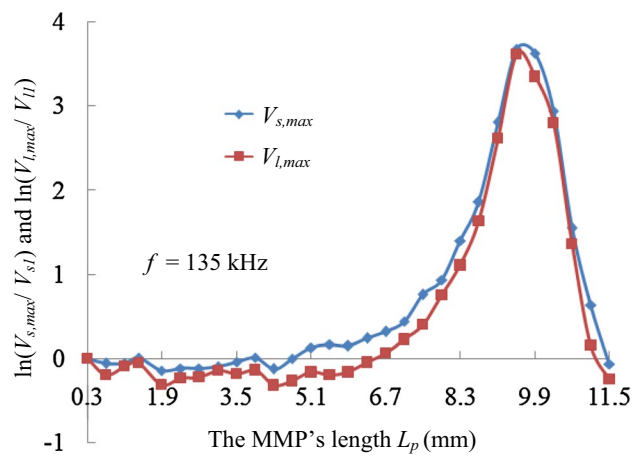


**Fig. 10** (color online). Acoustic streaming fields at different MMP's length  $L_p$  at 135 kHz. **a** Acoustic streaming patterns on the substrate surface and in the  $yz$  plane (the plane that is perpendicular to the substrate and vibration transmission needle, and passes the center axis of the MMP) at  $L_p = 0.3, 7$  and  $9.5$  mm. **b** The maximum acoustic streaming velocities on the substrate surface and in the  $yz$  plane versus the MMP's length. The *black circles* in images **a1, a3** and **a5**, representing the boundary between the fine and coarse element regions, have a radius of  $15 \mu\text{m}$ . And the *white zones* in images **a2, a4** and **a6**, representing the cross section of MMP, have a width of  $10 \mu\text{m}$



(a)



(b)

**Fig. 11** (color online). Acoustic streaming fields at different liquid film's thickness  $H$  at 135 kHz. **a** Acoustic streaming patterns on the substrate surface and in the  $yz$  plane (the plane that is perpendicular to the substrate and vibration transmission needle, and passes the center axis of the MMP) at  $H = 15, 50$  and  $300 \mu\text{m}$ . **b** The maximum acoustic streaming velocities on the substrate surface and in the  $yz$  plane versus the thickness of the liquid film. The *black circles* in images **a1, a3** and **a5**, representing the boundary between the fine and coarse element regions, have a radius of  $15 \mu\text{m}$ . And the *white zones* in images **a2, a4** and **a6**, representing the cross section of MMP, have a width of  $10 \mu\text{m}$

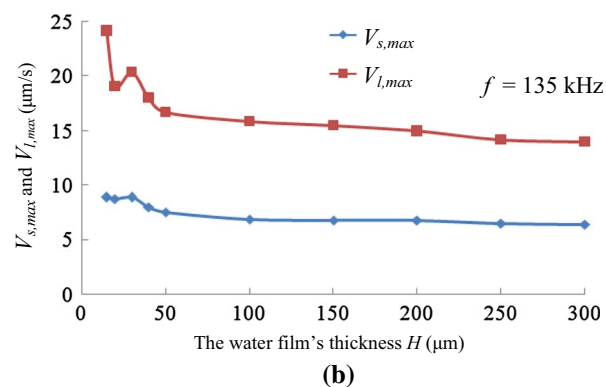
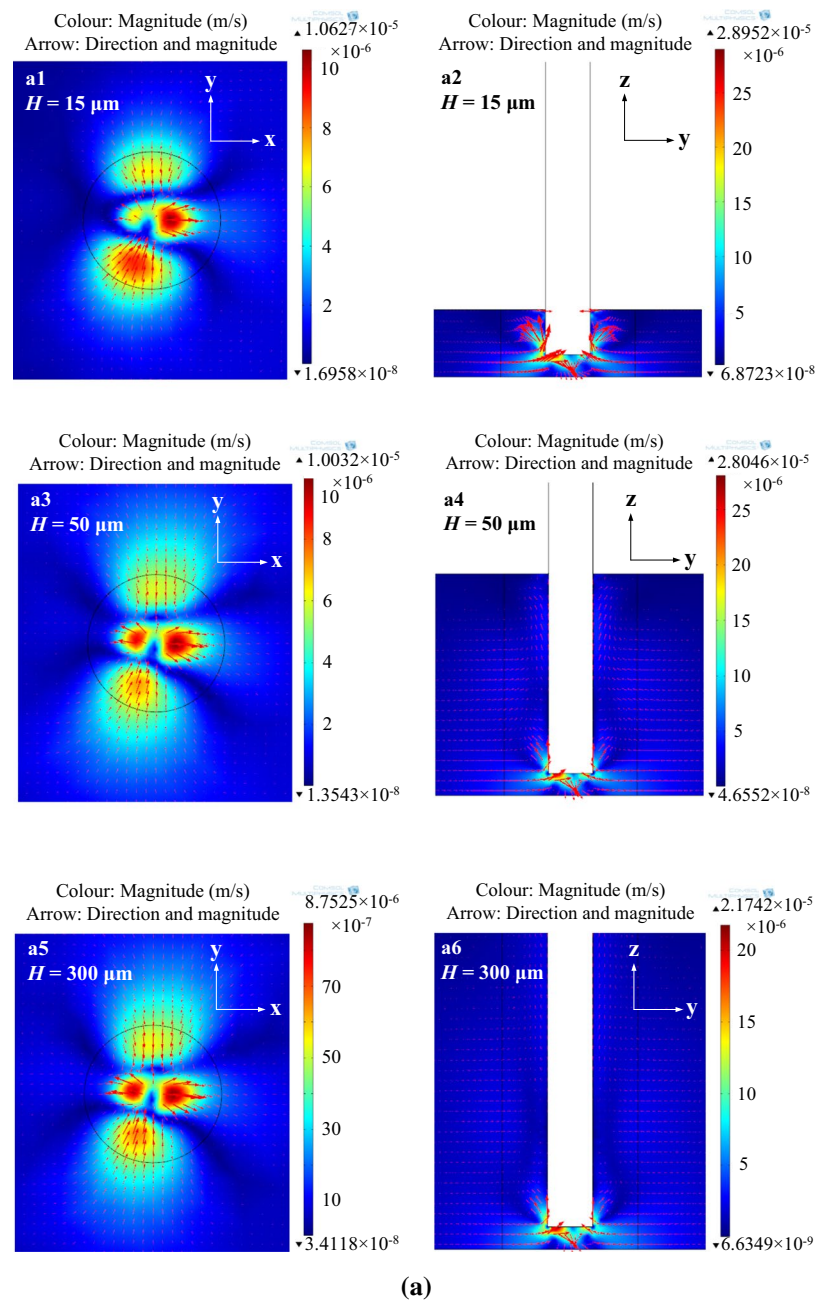


**Table 3** Effects of some dimensional parameters on the acoustic streaming field at 135 kHz

	The distance between the MMP tip and substrate $d_0$	The MMP’s radius $R_p$	The MMP’s length $L_p$	The water film’s thickness $H$
Acoustic streaming pattern	Affected	Affected	Insensitive	Insensitive
Acoustic streaming velocities	Affected	Sensitive near the MMP resonance point	Sensitive near the MMP resonance point	Insensitive for large $H$ ( $>50 \mu\text{m}$ )

frequency was 135 kHz, and the vibration excitation conditions listed in Table 2 were used. Figure 9a shows the acoustic streaming fields when the MMP’s radius is 1, 8 and 12  $\mu\text{m}$ , respectively, and Fig. 9b shows the change of  $V_{s,\text{max}}$  and  $V_{l,\text{max}}$  with the MMP’s radius. The vertical axis of Fig. 9b represents the natural logarithm of  $V_{s,\text{max}}/V_{s0}$  and  $V_{l,\text{max}}/V_{l0}$ , where  $V_{s0}$  ( $=0.05 \mu\text{m/s}$ ) and  $V_{l0}$  ( $=0.66 \mu\text{m/s}$ ) are the maximum acoustic streaming velocities on the substrate and along the  $z$  direction for an MMP’s radius of 1  $\mu\text{m}$ , respectively. From images a1 and a2, it is seen that when the MMP’s radius is too small, a nanowire on the substrate may be sucked to the MMP and then lifted, but it is difficult to trap the nanowire onto the MMP because it cannot rotate  $90^\circ$  during the lift process. Figure 9b shows that when the MMP’s radius is about 11.5  $\mu\text{m}$ , there is a large peak of acoustic streaming velocity. Our computation shows that this phenomenon is caused by a resonance of the MMP. If the working point was at the peak or very close to the peak, a disturbance such as the decrease in the water film thickness and an impact of micro-/nanoobject on the MMP would cause a substantial change of the acoustic streaming velocity around the MMP. Thus, the MMP’s radius should be so designed that the working point is not at the MMP’s resonance.

The effect of the MMP’s length on the acoustic streaming field was computed, and the results are shown in Fig. 10. In the computation, the working frequency was 135 kHz, and the vibration excitation conditions listed in Table 2 were used. Figure 10a shows the acoustic streaming fields when the MMP’s length is 0.3, 7 and 9.5 mm, respectively, and Fig. 10b shows the change of  $V_{s,\text{max}}$  and  $V_{l,\text{max}}$  with the MMP’s length. The vertical axis of Fig. 10b represents the natural logarithm of  $V_{s,\text{max}}/V_{s1}$  and  $V_{l,\text{max}}/V_{l1}$ , where  $V_{s1}$  ( $=6.84 \mu\text{m/s}$ ) and  $V_{l1}$  ( $=16.71 \mu\text{m/s}$ ) are the maximum acoustic streaming velocities on the substrate and along the  $z$  direction for the MMP’s length of 0.3 mm, respectively. From images a1, a2 and a3, it is seen that the MMP’s length affects the symmetry of the acoustic streaming field, which is caused by the change of phase difference  $\Phi_{zy}$  and  $\Phi_{zx}$ . Figure 10b shows that when the MMP’s length is about 9.9 mm, there is a large peak of acoustic streaming velocity. The computation shows that this phenomenon is caused by a resonance of the MMP. If the working point is at the peak, a disturbance such as the decrease in the water

film thickness and an impact of micro-/nanoobject on the MMP would cause a substantial change of the probe’s resonance frequency and the acoustic streaming velocity around the MMP. Thus, the MMP’s length should be so designed that the working point is not at the MMP’s resonance.

The dependency of the acoustic streaming field around the MMP on the water film’s thickness was computed at 135 kHz, and the results are shown in Fig. 11. In the computation, all of the parameters other than the water film’s thickness are kept constant. Figure 11a lists the acoustic streaming fields when the water film’s thickness is 15, 50 and 300  $\mu\text{m}$ , respectively. And Fig. 11b shows the maximum acoustic streaming velocities on the substrate  $V_{s,\text{max}}$  and along the  $z$  direction  $V_{l,\text{max}}$  versus the water film’s thickness. From Fig. 11a, it is seen that the asymmetry of the acoustic streaming field increases as the water film’s thickness decreases, which means that a thin water film may weaken the trapping capability. This is because as the water film’s thickness decreases, the spatial asymmetry of driving force  $F_j$  (see Eq. 3) of the acoustic streaming is amplified. From Fig. 11b, it is seen that when the water film is sufficiently thick, the water film’s thickness has little effect on the acoustic streaming velocities. This means that the acoustic streaming field for the nanowire trapping is mainly determined by the ultrasonic field near the substrate and MMP’s tip when the water film is sufficiently thick.

The effects of the working and size parameters on the pattern and velocity of the acoustic streaming field are summarized in Table 3.

### 5 Summary

We have numerically computed and analyzed the three-dimensional acoustic streaming field in the probe-liquid-substrate system, in which a MMP is inserted into a layer of nanosuspension film on a substrate. The computational results can well explain why the device works at some frequencies and does not work at others, and the computed acoustic streaming field agrees with the observed one very well. It is found that the phase difference and magnitude ratio among the orthogonal vibration components of the MMP root have a large effect on the symmetry of the acoustic streaming field, thus determining whether the

acoustic streaming field is usable in the contact-type trapping of a single nanowire. The MMP root's elliptical vibration perpendicular to the substrate can generate the acoustic streaming field capable of trapping a single nanowire in the contact mode. It is also found that the velocity and pattern of the acoustic streaming change with the distance between the MMP and substrate, the MMP's radius and length, and the water film's thickness.

**Acknowledgments** This work is supported by the following funding organizations in China: The National Basic Research Program of China (973 Program, Grant No. 2015CB057501), State Key Lab of Mechanics and Control of Mechanical Structures (0314G01), and PAPD.

## References

- Ahmed S, Gentekos DT, Fink CA, Mallouk TE (2014) Self-Assembly of nanorod motors into geometrically regular multimers and their propulsion by ultrasound. *ACS Nano* 8(11):11053–11060
- Balk AL, Mair LO, Mathai PP, Patrone PN, Wang W, Ahmed S, Mallouk TE, Liddle JA, Stavis SM (2014) Kilohertz rotation of nanorods propelled by ultrasound, traced by microvortex advection of nanoparticles. *ACS Nano* 8(8):8300–8309
- Beyer RT (1965) Nonlinear acoustics. In: Mason WP (ed) *Physical acoustics*, vol 2B. Academic Press, New York, pp 231–263
- Beyer RT (1997) The parameter B/A. In: Hamilton MF, Blackstock DT (eds) *Nonlinear acoustics: theory and applications*. Academic Press, New York, pp 25–39
- Devendran C, Gralinski I, Neild A (2014) Separation of particles using acoustic streaming and radiation forces in an open microfluidic channel. *Microfluid Nanofluid* 17(5):879–890
- Hu JH (2014) *Ultrasonic micro/nano manipulations*. World Scientific Publishing, Singapore
- Kinsler LE, Frey AR, Coppens AB, Sanders JV (1999) *Fundamentals of acoustics*. Hamilton Press, Te Rapa
- Lei J, Hill M, Glynn-Jones P (2014) Numerical simulation of 3D boundary-driven acoustic streaming in microfluidic devices. *Lab Chip* 14(3):532–541
- Li HQ, Hu JH (2014a) Noncontact manipulations of a single nanowire using an ultrasonic microbeak. *IEEE Trans Nanotechnol* 13(3):469–474
- Li N, Hu JH (2014b) Sound controlled rotary driving of a single nanowire. *IEEE Trans Nanotechnol* 13(3):437–441
- Li N, Hu JH, Li HQ, Bhuyan S, Zhou YJ (2010) Mobile acoustic streaming based trapping and 3-dimensional transfer of a single nanowire. *Appl Phys Lett* 101(9):093113
- Liebermann LN (1949) The second viscosity of liquids. *Phys Rev* 75:1415–1422
- Lighthill J (1978) Acoustic streaming. *J Sound Vib* 61(3):391–418
- Muller PB, Barnkob R, Jensen MJH, Bruus H (2012) A numerical study of microparticle acoustophoresis driven by acoustic radiation forces and streaming-induced drag forces. *Lab Chip* 12(22):4617–4627
- Muller PB, Rossi M, Marin AG, Barnkob R, Augustsson P, Laurell T, Kaehler CJ, Bruus H (2013) Ultrasound-induced acoustophoretic motion of microparticles in three dimensions. *Phys Rev E* 88(2):023006
- Nama N, Huang PH, Huang TJ, Costanzo F (2014) Investigation of acoustic streaming patterns around oscillating sharp edges. *Lab Chip* 14(15):2824–2836
- Sundin SM, Jensen TG, Bruus H, Kutter JP (2007) Acoustic resonances in microfluidic chips: full-image micro-PIV experiments and numerical simulations. *Lab Chip* 7(10):1336–1344
- Tang Q, Hu JH (2015) Diversity of acoustic streaming in a rectangular acoustofluidic field. *Ultrasonics* 58:27–34
- Wada Y, Koyama D, Nakamura K (2014) Acoustic streaming in an ultrasonic air pump with three-dimensional finite-difference time-domain analysis and comparison to the measurement. *Ultrasonics* 54(8):2119–2125
- Zhou YJ, Hu JH, Bhuyan S (2013) Manipulations of silver nanowires in a droplet on low-frequency ultrasonic stage. *IEEE Trans Ultrason Ferroelectr Freq Control* 60(3):622–629